International Journal of Technology

http://ijtech.eng.ui.ac.id

Research Article

Physicochemical and Mechanical Evaluation of Freeze-Dried Hydroxyapatite–β-Tricalcium Phosphate–Polycaprolactone–Copper–Zinc Scaffolds

Theophani Orlee Cahyadi[1], Devina Novelia[1], Natasya Maharani Putri Sidharta[1], Mora Octavia[2*], Tena Djuartina[3], Evi Ulina Margareta[4], Widodo Widjaja Basuki[5], Ferry Rippun Gideon Manalu[6], Daniel Edbert[7]

[1]Bachelor of Medicine Study Programme, School of Medicine and Health Sciences, Atma Jaya Catholic University of Indonesia, Jl. Pluit Raya No. 2, North Jakarta 14440, Indonesia

[2]Department of Dental Medicine, School of Medicine and Health Sciences, Atma Jaya Catholic University of Indonesia, Jl. Pluit Raya No. 2, North Jakarta 14440, Indonesia

[3]Department of Anatomy, School of Medicine and Health Sciences, Atma Jaya Catholic University of Indonesia, Jl. Pluit Raya No. 2, North Jakarta 14440, Indonesia

[4]Department of Physiology, School of Medicine and Health Sciences, Atma Jaya Catholic University of Indonesia, Jl. Pluit Raya No. 2, North Jakarta 14440, Indonesia

[5]Master's Program in Mechanical Engineering, School of Bioscience, Technology, and Innovation (SBTI), Atma Jaya Catholic University of Indonesia, Jl. Raya Cisauk Lapan, Banten 15345, Indonesia

[6]Electrical Engineering Study Program, School of Bioscience, Technology, and Innovation (SBTI), Atma Jaya Catholic University of Indonesia, Jl. Raya Cisauk Lapan, Banten 15345, Indonesia

[7]Department of Microbiology, School of Medicine and Health Sciences, Atma Jaya Catholic University of Indonesia, Jl. Pluit Raya No. 2, North Jakarta 14440, Indonesia

*Corresponding author: mora.octavia@atmajaya.ac.id; Tel.: +6221-669-4366; Fax.: +6221-660-6123

Abstract: Bone graft materials are essential for supporting alveolar bone regeneration, particularly in patients with periodontitis who require improved mechanical stability of bone graft scaffold in load-bearing regions. This study aimed to develop and characterize a biphasic bone graft scaffold composed of hydroxyapatite (HAp, 60%) and β-tricalcium phosphate (β-TCP, 40%) combined with poly(ϵ-caprolactone) (PCL) and reinforced with copper (Cu) and zinc (Zn) bioactive ions. The scaffold was fabricated using dimethylformamide (DMF) as the solvent through a freeze-drying process and subsequently compared with a xenograft control. Fourier-transform infrared spectroscopy confirmed the presence of inorganic phosphate groups and organic ester linkages, while the disappearance of the characteristic dimethylformamide (DMF) peak verified the effective solvent removal. X-ray diffraction analysis revealed that calcium phosphorus oxide (86.73%) was the dominant phase and calcium hydrogen phosphate (13.26%) was the secondary phase, indicating that DMF influenced both phase formation and crystallinity. The resulting scaffold exhibited lower porosity (36.39%) than the control (95.79%) but demonstrated substantially higher compressive strength (3.873 MPa) and yield strength (3.024 MPa) than the control (0.980 MPa and 0.537 MPa, respectively). However, water absorption (37.7%) and blood absorption (29.1%) were reduced relative to the control group. Overall, these findings indicate that the HAp–β-TCP–PCL-Cu-Zn scaffold (tested specimen) fabricated using DMF provides enhanced structural stability and crystallinity, supporting its potential use in load-bearing bone regeneration applications.

Keywords: Freeze-drying; Mechanical evaluation; Periodontitis; Physiochemical characterization; Porosity

https://doi.org/10.14716/ijtech.v17i3.8261
Received November 2025; Revised January 2026; Accepted April 2026

1. Introduction

Periodontal disease is a chronic multifactorial inflammatory disease characterized by progressive destruction of periodontal ligaments and alveolar bone. Majority of the pathogens are associated with Gram-negative anaerobic pathogens, such as *Porphyromonas gingivalis*, *Tannerella forsythia*, and *Treponema denticola* (Kwon et al., 2020). The risk factors include type 2 diabetes mellitus and smoking, which increase the susceptibility of individuals (Hajishengallis and Chavakis, 2021). In Indonesia, the prevalence of periodontitis reached 74.1% according to Riset Kesehatan Dasar (Riskesdas) in 2018 (Badan Penelitian dan Pengembangan Kesehatan, 2020), whereas the World Health Organization (WHO) reports more than one billion cases of severe periodontal disease globally (Jain et al., 2023). This condition leads to alveolar bone absorption and tooth loss if left untreated, emphasizing the need for effective regenerative therapies (Gasner and Schure, 2023).

Bone grafts are widely used to restore alveolar bone defects and support periodontal regeneration. An ideal bone graft requires three fundamental biological properties: osteogenesis, osteoconduction, and osteoinduction (Zhao et al., 2021). Osteoconduction provides a structural framework that facilitates the migration and growth of new bone tissue within the microarchitecture of the scaffold. Osteoinduction complements this by initiating the differentiation of progenitor cells into osteoblasts through bioactive mediators such as bone morphogenetic proteins (BMPs). Osteogenesis represents the cellular phase of new bone formation, in which these differentiated osteoblasts mineralize the bone matrix (Keum et al., 2023). Bone grafts are classified into natural, autografts, allografts, xenografts, and synthetic grafts. Autografts are the gold standard; however, synthetic grafts made of hydroxyapatite ($Ca_{10}(PO_4)_6(OH)_2$; HAp) and/or beta-tricalcium phosphate ($Ca_3(PO_4)_2$; β-TCP) are increasingly preferred due to their non-immunogenic nature and lower risk of morbidity (Zhao et al., 2021). However, it contains no antibacterial component and has significantly low mechanical strength especially β-TCP due to its fast absorption ability (Chauhan et al., 2009), which induces a scaffold's osteoconductive property compared to HAp, which has more of a crystalline structure reflecting its osteoconductive property (Hashimoto et al., 2024).

The application of bone graft scaffold to alveolar socket preservation procedure and the need to preserve the dimension of the alveolar ridge while maintaining cell growth within the area are urgently required to enhance mechanical strength. Therefore, the ratio of HAp ceramics will be higher than that of β-TCP ceramics (Prasadh and Wong, 2018; Raja et al., 2022). In addition to mechanical performance, biological properties such as water and blood absorption capacity are crucial because postoperative bleeding can occur during tooth extraction procedures. Bone grafts that also act as hemostatic sponges can help minimize bleeding and promote the regeneration process (Rozykulyyeva et al., 2025).

Other materials will also be added into making the bone graft scaffold, namely poly ϵ-caprolactone (PCL), copper (Cu) and zinc (Zn). According to a study conducted by Dwivedi et al., 2020, among other polymers, PCL tends to degrade the slowest, reflecting its superior mechanical properties and could enhance stability of scaffold made (Dwivedi et al., 2020). Besides, trace elements such as Cu and Zn could help enhance antimicrobial and osteogenic potential that offers clinically feasible periodontal bone graft scaffolds (Tan et al., 2021; Wen et al., 2023). These findings have made positive contributions toward the scaffold produced; however, it has yet to be incorporated all together in a biphasic scaffold. Hence, this research will see whether it affects the scaffold's characteristics.

ShiraliPour et al., 2021 used a freeze-drying technique to produce β-TCP-PCL bone graft scaffold that appears to have better porosity without using porogens. Moreover, the addition of PCL has been reported to improve the mechanical strength (Lv et al., 2024; ShiraliPour et al., 2021). Freeze-drying is a promising method for scaffold fabrication as incorporating low temperature helps preserve heat-sensitive polymers such as PCL, reducing shrinkage, maintaining a better shape of the produced scaffold, and producing high porosity that increases its interconnectivity (Purnaning et al., 2025). PCL is a high-molecular-weight polymer that requires

a high-molecular-weight solvent such as dimethylformamide (DMF) (Aboudzadeh et al., 2021). Although it is considered to be toxic to the human body, it can be removed during the freeze-drying process (ShiraliPour et al., 2021). In addition to the solvent's ability to dissolve PCL, DMF has a slow evaporation rate that could produce a denser scaffold that could enhance its mechanical properties (Choudhury et al., 2015; Omiyale et al., 2025) supported this finding, stating that various solvents have different evaporation rates and chain flexibility, leading to different densities. For example, dichloromethane (DCM) dissolves polylactic acid (PLA) with its characteristic fast evaporation and rigid chain. This leads to a more porous and less dense scaffold. (Choudhury et al., 2015). Thus, this would be the opposite of the DMF used in this research. The decision to incorporate PCL instead of other polymers, such as PLA, is due to the higher water uptake and possibly better bone-regeneration ability with similar mechanical strength that is accepted for bone graft scaffold (Cheng et al., 2021). In addition, PCL has a longer degradation rate (1–3 years) than PLA (6–9 months) (Basoz et al., 2024; Capuana et al., 2022; Ghezzi et al., 2024), allowing complete regeneration and remodeling of bone tissue that takes approximately 12 months (Ghezzi et al., 2024). Concerns about the slow degradation rate of PCL are addressed by the presence of other resorbable ceramic phases, such as HAp and β-TCP (several weeks to several months) (Veiga et al., 2023) that could balance its degradation rate, resulting in a composite with a more physiologically appropriate degradation profile with better mechanical strength.

This study aims to investigate the influence of DMF-assisted freeze-drying on the physicochemical and mechanical characteristics of a 60:40 HAp–β-TCP–PCL–Cu–Zn composite scaffold. The work is positioned at the material validation stage, emphasizing structural integrity, phase composition, crystallinity, porosity, and functional absorption behavior before biological evaluation. A commercially available xenograft derived from bovine bone was used as a benchmark reference to contextualize the material performance within clinically accepted ranges. The xenograft composition (calcium: 31.32%, phosphorus: 14.10%) (Taufik et al., 2017) closely resembles that of human bone (calcium: 24.5%, phosphorus: 11.5%) (Kono et al., 2022), providing a relevant comparative standard for guided bone regeneration applications.

Although biphasic calcium phosphate–polymer composites have been widely reported, few studies have systematically evaluated a DMF-processed HAp–β-TCP scaffold with a 60:40 ratio reinforced by Cu–Zn trace elements and correlated its phase evolution, mechanical performance, and absorption characteristics within a unified framework. Therefore, the novelty of this work lies in integrating composition and solvent-driven processing strategy to examine the composite scaffold's structure–property relationship. Comprehensive characterization—including FTIR, XRD, porosity assessment, mechanical testing, and absorption analysis—was conducted to determine whether the proposed formulation achieves a balanced trade-off between mechanical competence and functional fluid interaction, supporting its potential application in guided bone regeneration.

2. Methods

2.1 Ethical Clearance

Ethical clearance (Approval No. 04/05/KEP-FKIKUAJ/2025) was obtained from the Ethical Committee for Medical Research of the School of Medicine and Health Sciences, Atma Jaya Catholic University—dr. Linda Suryakusuma, MA, Sp. S. as the head of the Ethics Committee.

2.2 Fabrication of Biphasic Calcium Phosphate Bone Graft Scaffold

Scaffolds were fabricated using Poly ϵ-caprolactone (~3mm pellets, average MN 80.000) (Merck, Darmstadt, Germany) dissolved in N,N-dimethylformamide (Merck, Darmstadt, Germany) in a 1:10 ratio, combined with hydroxyapatite (HAp, 0.5-1.0 mm particle size) (912190-Sigma Aldrich, Germany) and β-TCP (unsintered powders obtained from Sigma-Aldrich, Germany) in a 60:40 ratio, combined with trace copper (<63 µm) (1.02703.0250, Merck, Darmstadt,

Germany) and zinc (<45 µm) (Merck, Darmstadt, Germany) (0.1 wt.% in a 50:50 ratio). HAp granules were ground in advance and pre-suspended with nitric acid:DMF (1:2:1) before mixing. Mixing was performed using a magnetic stirrer (50°C; 300 rpm). The mixtures were cast into molds, frozen at 80°C for 6 days, and then freeze-dried (55°C) for 48 h to remove residual solvents. The samples were vacuum-dried and incubated at 25°C for 7 days. The produced bone graft scaffold will be used as a test specimen and compared with a commercial xenograft bone graft scaffold (BATAN® Xenograft, Bogor, Indonesia) as a control specimen. Each measurement test was conducted once for every sample, and data reliability was ensured using calibrated equipment, identical preparation protocols, and controlled experimental conditions.

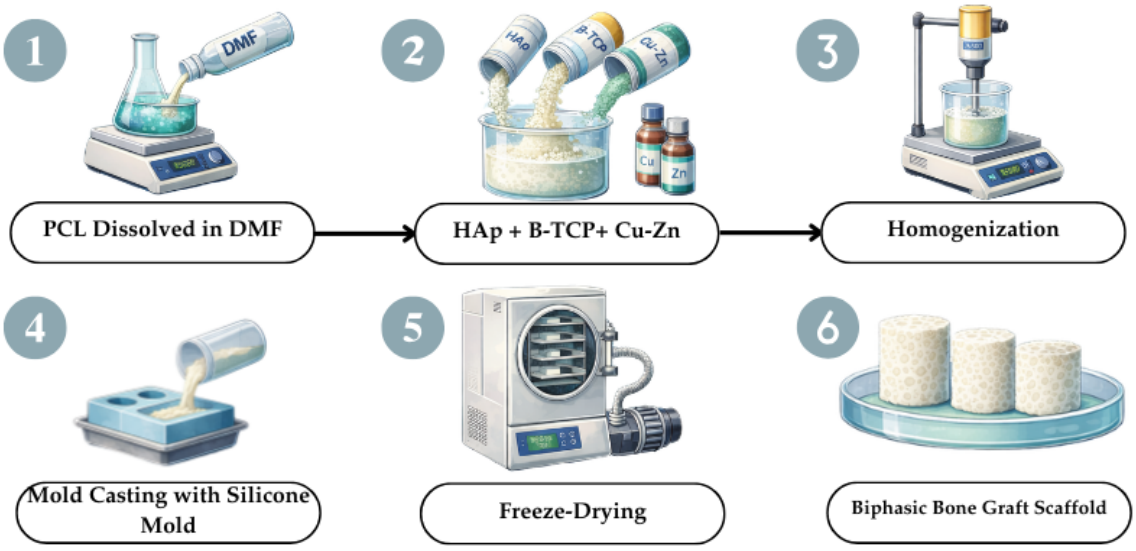

Figure 1 Schematic of the fabrication process of HA_p-β-TCP-PCL-Cu-Zn scaffolds

2.3 Characterization and Evaluation of Bone Graft Scaffolds

2.3.1 Fourier transform infrared FTIR (Fourier Transform Infrared)

The chemical composition of the scaffold samples was examined using an IRTracer-100 spectrometer (Shimadzu, Kyoto, Japan) integrated with LabSolutions IR analytical software (Shimadzu, Kyoto, Japan). The Attenuated Total Reflectance (ATR was applied to identify specific functional moieties of organic and inorganic origin within the material. Spectral measurements were obtained across the 4000–400 cm^{-1} range, and the resulting absorption bands were correlated with the characteristic vibrational frequencies described in a previous studies.

2.3.2 X-ray diffraction

Powdered scaffold samples were mounted on aluminum sample stages and flattened gently using a glass slide to ensure a uniform surface. X-ray diffraction (XRD) analysis was performed using a Malvern Panalytical X'Pert PRO diffractometer (Malvern Panalytical, Almelo, Netherlands) over a specified 2θ scanning interval. The obtained diffraction profiles were processed and interpreted using X'Pert Quantify software (Malvern Panalytical, Almelo, Netherlands), and the crystalline phases were determined by comparing them with reference patterns from the International center for Diffraction Data (ICDD) database.

2.3.3 Archimedes Principle

Archimedes' principle assesses the scaffold porosity using the liquid displacement method. This test was performed by preparing a 10 x 10 mm scaffold that will be submerged in phosphate-

buffered saline, and its weight (m_{sub}) will consequently be measured with an analytical balance ACJ 200-4M (Kern and Sohn, Balingen, Southern Germany). Afterwards, the scaffold was submerged for 15 minutes and measured its saturated weight (m_{sat}). Then, the scaffold will be vacuum-dried at 27°C for 24 h, and its mass will be weighed (m_{dry}). The scaffold's open porosity (γ,%) will be calculated as follows (Equation 1) (Jang and Ahn, 2023):

$$\gamma(\%) = \frac{m_{sat} - m_{dry}}{m_{sat} - m_{sub}} \times 100 \quad (1)$$

2.3.4 Light Microscopy

Each bone graft scaffold will be analyzed using an Olympus CX-23 light microscope (Olympus Corporation, Tokyo, Japan) to assess its morphology, macropore dimensions and surface architecture. Observations were performed at 10x magnification, and digital micrographs were acquired for subsequent evaluation. ImageJ software (National Institutes of Health, Bethesda, MD, USA) was used to process the images and determine pore diameter and distribution by measuring five different pores within the specimen and obtaining its average.

2.3.5 Scanning electron microscope (SEM)

Scanning electron microscopy (JEOL JSM-6510LA, JEOL Ltd., Tokyo, Japan) was used to investigate the microscopic architecture of the bone graft scaffolds to obtain detailed visualization of surface features and internal microporosity. Each specimen was trimmed into pieces of approximately 10 × 10 mm, securely placed on aluminum holders using carbon adhesive tape, and subsequently gold-coated by sputter deposition to enhance conductivity. Imaging was conducted using a JEOL JSM-6510LA microscope (JEOL Ltd., Tokyo, Japan) operating at an accelerating voltage of 10 kV, with micrographs acquired at magnifications between 1.000× and 25.000× and the pore size was measured using ImageJ Software (National Institutes of Health, Bethesda, USA). The pore size was determined by measuring five different pores within the specimen and obtaining its average.

2.3.6 Mechanical Testing

Mechanical tests were conducted with a universal testing machine (BSD Campus UNIKA Atma Jaya, BSD, Indonesia) at a crosshead speed of ±10 µm/s and maximum load of 20.25 kN with an output sensitivity of 1.996 mv/v and comprehensive error of <0.5% F.S (Manalu and Basuki, 2025). The ultimate compressive strength and yield strength were calculated from stress-strain curves in Megapascal units. The ultimate compressive strength is obtained by identifying the maximum value of stress given to a material, whereas the yield strength (σ_y) is obtained by creating two perpendicular lines following thecurve's shape and identifying its meeting point (Callister and Rethwisch, 2020).

2.3.7 Water Absorption

Scaffolds (10 × 10 mm) were weighed (W_0), immersed in 20 mL deionized water for 60 min at room temperature (25°C), blotted dry, and reweighed (W_t). Water absorption (%) was calculated using Equation (2):

$$Q(\%) = \frac{W_t - W_o}{W_o} \times 100 \quad (2)$$

The result will determine whether the bone graft scaffold can attract fluids that could facilitate the growth and cell differentiation of the alveolar bone (Rozykulyyeva et al., 2025).

2.3.8 Blood absorption and adhesion

This test reflects how well a scaffold can form a matrix that supports the migration and infiltration of osteoprogenitor cells, as well as the transport of growth factors such as VEGF, which are essential for alveolar bone regeneration. Each specimen will be cut into 10 mm x 10 mm pieces. Consequently, 200 µL of fresh sheep blood, which was initially mixed with 3.8% sodium citrate solution, was dropped onto each specimen and left for an hour to determine how much blood was absorbed. The specimens were measured for their initial weight (D_0) and weight after blood absorption (D_t) and documented. The blood absorption capacity was measured as follows (Equation 3):

$$Dx(\%) = \frac{D_t - D_o}{D_o} \times 100 \tag{3}$$

Each specimen was placed inside a test tube filled with 40% phosphate-buffered saline (PBS), shaken 10x, and documented for its blood adhesion test (Rozykulyyeva et al., 2025).

3. Results and Discussion

3.1 Morphological analysis of the bone graft scaffolds

Based on the produced bone graft scaffold shown in Figure 2, its morphology showed inhomogeneity as it did not result in the expected spongy surface; however, it contains hard surfaces. The top surface of the bone graft scaffold in Figure 2a is a light green hard surface surrounded by spongy material, whereas its bottom surface in Figure 2b is a cyan surface with a hard texture. The produced bone graft scaffold is hard but brittle when being cut for further evaluations, and it has also experienced shrinking in the freeze-drying process.

In contrast to the produced bone graft scaffold, Figure 2c shows the off-white color of the control specimen with homogenous pores that are visible macroscopically. The texture of the control specimen is hard and not brittle when cut for further analysis.

The fabricated bone graft scaffold exhibited morphological inhomogeneity, as evident in the bottom surface where copper deposition was observed. This phenomenon may be attributed to the chemical structure of dimethylformamide (DMF, C_3H_7NO). DMF contains a carbonyl (C=O) group that acts as a strong oxygen donor, oxidizing copper and producing a blue coloration. Furthermore, hydroxyapatite contains hydroxyl (–OH) groups, whereas β-tricalcium phosphate does not. DMF and HAp are considered good ligands (Mondal et al., 2023; Muzart, 2009) that induce ligand-field effects in addition to oxidation, leading to d-orbital splitting and the characteristic blue color (Kumar, 2024). Another limitation of the tested specimen was its tendency to shrink, which is not associated with ligand-field effects but rather with the inherent properties of DMF. Because DMF does not readily crystallize or form a complete lattice structure during the freezing stage at 80°C, the subsequent freeze-drying process produces stress within the pore walls as the solvent does not uniformly sublimate, resulting in structural shrinkage (Ratajczyk et al., 2018). Additionally, its dense structure could also be due to the higher percentage of HAp as has been reported by Lee et al., 2022 that the increasing amount of HAp will result in higher mechanical properties as well as higher surface hardness, however its drawbacks being its inverse nature with porosity properties (Lee et al., 2022). Hence, it will be discussed further.

3.2 Fourier transform infrared (FTIR) and X-ray diffraction (XRD)

As shown in Figure 3, the trend spectrum of the produced bone graft scaffolds for both the white and bottom surfaces showed similar results in terms of peak wavelength and interpretation of the stretching and functional groups.

The control specimen in Figure 3c has slight differences with the produced bone graft scaffold in Figures 3a and 3b, as it is known to be demineralized bovine bone; its process

removed most of the organic components while preserving the inorganic components such as hydroxyapatite. Ragu et al., 2015 reported that xenografts such as Bio-Oss and Gen-Os contain collagenous components, hydroxyapatite, and natural bone proteins (Ragu et al., 2015). The distinct bands at 1543 cm^{-1} and 1651 cm^{-1} represent amide II and amide I, respectively. Amide is a type I collagen moiety characterized by its C-N-H and C=O bond (Figueiredo et al., 2012).

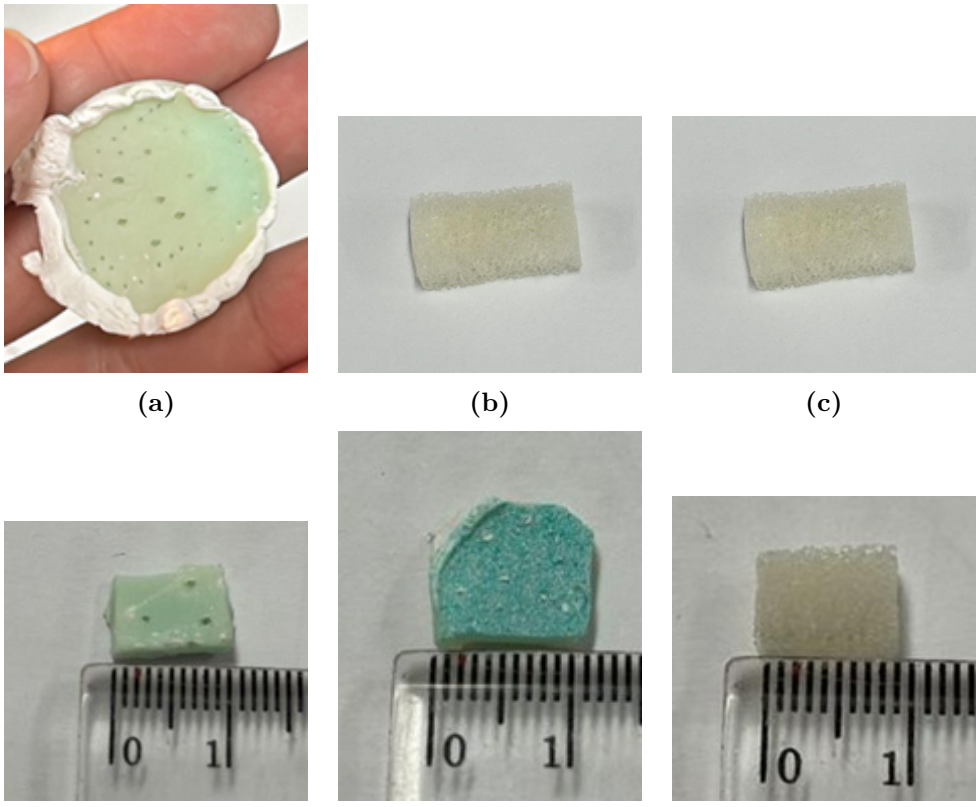

Figure 2 Morphology of the samples. (a) Top surface of the tested specimen after freeze-drying, (b) bottom surface of the tested specimen after freeze-drying, (c) control specimen, (d) top surface of the tested specimen with a width of 1 cm, (e) bottom surface of the tested specimen with a width of 1.1 cm, and (f) control specimen with a width of 0.9 cm

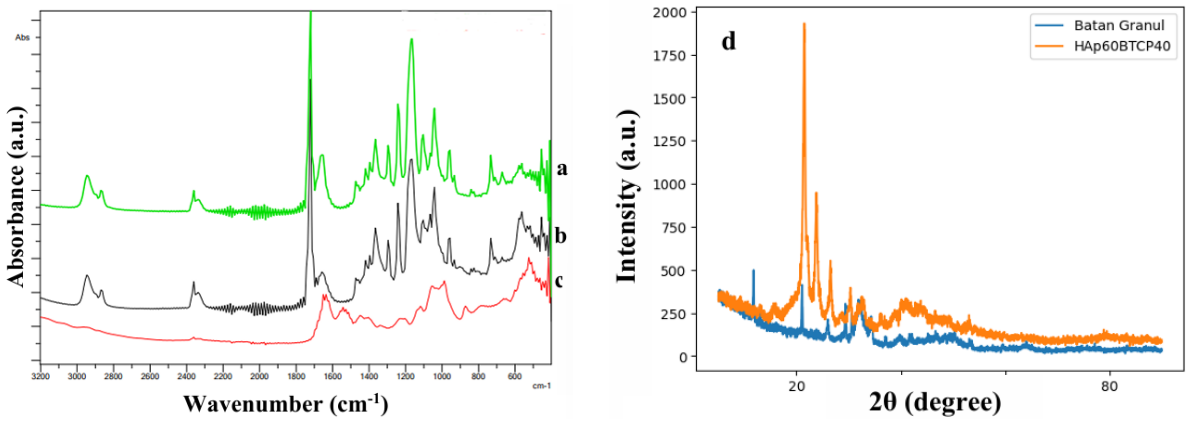

Figure 3 FTIR spectrum and XRD of the produced bone graft scaffolds and control specimen. (3a) FTIR spectrum of the white surface of the bone graft scaffold, (3b) FTIR spectrum of the bottom surface of the bone graft scaffold, (3c) FTIR spectrum of control specimen and (3d) XRD of the tested and control specimens

The main difference between the produced bone graft scaffold and the ester groups and the

polymer backbone reflects the incorporation of PCL in the scaffold. PCL is a biodegradable polyester (Ntrivala et al., 2025); hence, the presence of an ester group is seen through the bands 1165-1242 cm^{-1} indicating C-O-C stretching, as well as 1720 cm^{-1} indicating C=O stretching of the ester. In addition, similar peaks showing the presence of inorganic compounds such as HAp/β-TCP is seen through the phosphate group (PO_4^{3-}) by its bands at various stretching vibrations characterized as ν_1-ν_4. The first stretching vibration was found at 957-987 cm^{-1} as symmetrical stretching, followed by ν_2 at 416-455 cm^{-1} and ν_4 at 524-563 cm^{-1} as bending vibrations, and ν_3 at 1041-1057 cm^{-1} as asymmetrical stretching. This confirms the presence of inorganic compounds within the BGS (Figueiredo et al., 2012).

The absence of the characteristic DMF band at 1670 cm^{-1} in the spectra of DMF-based scaffolds indicates that almost no residual DMF remained after freeze-drying. Overall, the FTIR analysis verified the presence of both inorganic functional groups (phosphate from HAp/β-TCP) and organic groups (C=O and C–O–C from PCL).

The crystalline composition of the fabricated bone graft scaffolds was examined using X-ray diffraction (XRD). This technique enabled the identification of major crystalline phases and assessment of how variations in HAp/β-TCP ratio and solvent type on phase formation. Phase matching and verification were conducted using the International Centre for Diffraction Data (ICDD) reference database. Figure 3d demonstrates the result of the assessment, which is related to the peak intensity.

Further peak analysis indicated that the main diffraction peaks for all groups appeared consistently in the 2θ range of 21–26°, with varying relative intensities. The tested specimen exhibited the sharpest diffraction pattern with a main peak at 21.47° (100% relative intensity) and secondary peaks at 23.77° (34.47%), 22.13° (17.55%), 21.42° (16.10%), and 23.83° (14.33%). The control group showed the highest peak at 21.02° (100% relative intensity) and secondary peaks at 11.73° (88.38%), 29.35° (66.04%), 30.59° (53.42%), and 34.21° (37.44%). This shows that as the tested specimen demonstrated sharper peaks overall, suggests that it has a high degree of crystallinity as well as a more structured order compared to the control specimen, which leans more to have a less uniform crystalline profile, hence, theoretically would have a better mechanical strength (Wang et al., 2017).

Through its crystalline phase analysis, the tested specimen presented two crystalline phases, namely, calcium phosphorus oxide (CaPO4) as the major phase (86.73%) and calcium hydrogen phosphate ($CaHPO_4$) as the minor phase (13.26%). The control specimen also showed two different phases, namely, hydroxyapatite as the major phase (63.36%) and brushite as the minor phase (36.64%).

The presence of two phases in the tested specimen indicates that DMF influences not only the dissolution of PCL but also the stability and phase formation of calcium phosphates. The occurrence of $CaHPO_4$, which has a lower Ca/P ratio and higher solubility than HAp or β-TCP, indicates that DMF promotes the formation of more soluble calcium phosphate phases.

Taken together, the results confirmed that both the control and tested specimens consisted of biphasic calcium phosphate structures. However, differences in the dominant crystalline species revealed that the solvent type significantly affected the phase stability and transformation. The tested specimen predominantly formed calcium phosphorus oxide with minor $CaHPO_4$, indicating partial phase conversion toward more soluble calcium phosphate species. This shift indicates that DMF facilitates ion mobility and alters the recrystallization environment during scaffold formation. The sharper and more intense diffraction peaks further reflect enhanced crystallinity in the tested specimen compared with the control, implying a more ordered crystal lattice and potential improvement in mechanical integrity.

3.3 Porosity (Archimedes principle, light microscopy, and scanning electron microscopy) and absorption capacity

The porosity analysis based on Archimedes' principle (Figure 4a) shows a significant difference between the control and tested specimens, with porosity values of 95.79%±4.79% and

36.39%±1.82% as calculated (Equation 4 and 5), respectively. The exceptionally high porosity of the control xenograft reflects the intrinsic characteristics of natural bone-derived materials, which retain the complex 3D trabecular architecture of cancellous bone after deproteinization and sintering.

The porosity testing results for the Archimedes principle shown in 4a are as follows:

$$\text{Control Specimen } \gamma(\%) = \frac{0.3075 - 0.0392}{0.3075 - 0.0274} \times 100 = 95.79\% \tag{4}$$

$$\text{Tested Specimen } \gamma(\%) = \frac{0.2210 - 0.1920}{0.2210 - 0.1413} \times 100 = 36.39\% \tag{5}$$

In contrast, the tested specimen exhibited substantially lower porosity. This reduced value can be attributed to the physicochemical properties of DMF as the solvent used during the scaffold fabrication process. DMF possesses a freezing point of -61°C which could have caused incomplete crystallization of the solvent or melting of the solvent when placed in the freeze dryer at -55°C. DMF also possesses a high polarity and slow evaporation rate (1.14 ml/min) (NOAA, n.d.), which can cause incomplete sublimation during freeze-drying. Consequently, pore walls tend to collapse due to capillary tension, leading to a denser microstructure with fewer open pores. Although the porosity of the tested specimen does not meet the ideal porosity of an ideal bone graft scaffold (>80%) (ShiraliPour et al., 2021), it could offer an advantage in terms of mechanical strength, as denser structures typically exhibit higher compressive resistance.

Figures 4b and 4c show a clear morphological difference between the control and tested specimens when observed under a light microscope at 10× magnification. The control specimen displays well-defined macropores that are generally round to oval in shape, with diameters ranging from 858 μm to 2221 μm with an average size of 2539 ± 2047 μm. However, compared to its ideal range of 250-400 μm, it is quite above the expected range. In contrast, the tested specimen exhibits a markedly different surface morphology dominated by hydroxyapatite (HAp) crystallites, visible as black granules, and copper (Cu) particles, observed as blue granules distributed unevenly across the scaffold surface.

The black granules are attributed to HAp because of its higher degree of crystallinity compared to β-TCP. Unlike in the control, distinct macropores are not clearly observed in this sample. Small intercrystalline voids and microgaps can be observed between the granules, indicating partial pore collapse during the freeze-drying process. This observation supports the previously obtained low porosity value (36.39%), indicating that the use of DMF as a solvent leads to a denser microstructure with limited pore interconnectivity. The blue coloration indicates the oxidation of copper due to the presence of DMF, as mentioned in the morphological analysis.

The SEM micrographs in Figures 4d and 4e show distinct morphological differences between the two scaffolds at 15,000x magnifications. The control exhibited a relatively smooth and dense surface at lower magnifications (1000× & 5000×), characterized by elongated depressions measuring approximately 3–5 μm. At higher magnifications (10,000× & 15,000×), these depressions appeared as fibrillar-like networks with interconnecting micropores smaller than 1 µm.

The tested specimen displayed a highly porous and interconnected structure with irregular pore distribution and variable pore sizes, forming a continuous fibrillar network. The microstructure consisted of elongated, flexible, and overlapped polymer fibers of varying thicknesses, creating a mesh-like arrangement. This fibrillar morphology can be attributed to the use of DMF as the solvent, whose low volatility and polar nature promote polymer chain alignment through dipole–dipole and hydrogen bonding interactions with the ester groups of PCL (Obregon et al., 2016). Such interactions facilitate fiber formation and stabilize the pore network during freeze-drying, as also reported by Alberto et al., 2023 in electrospinning studies. According to Abbasi, 2020, pores smaller than 10 μm increase the surface area, thereby enhancing ion exchange, protein adsorption, and osteogenic cell attachment (Abbasi, 2020). Therefore, the

fibrillar and microporous architecture observed in the tested specimen is favorable for promoting cell adhesion and bone tissue ingrowth.

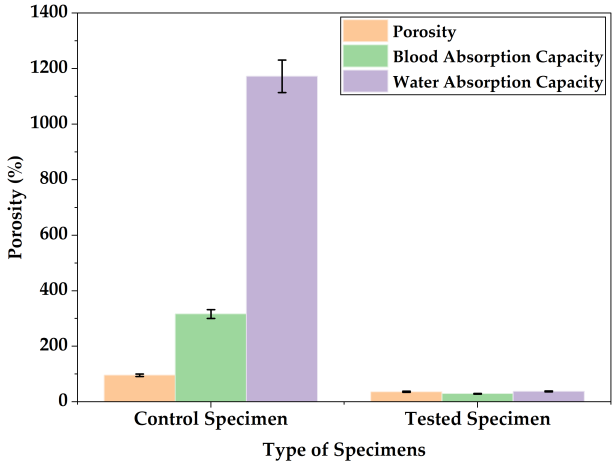

(a)

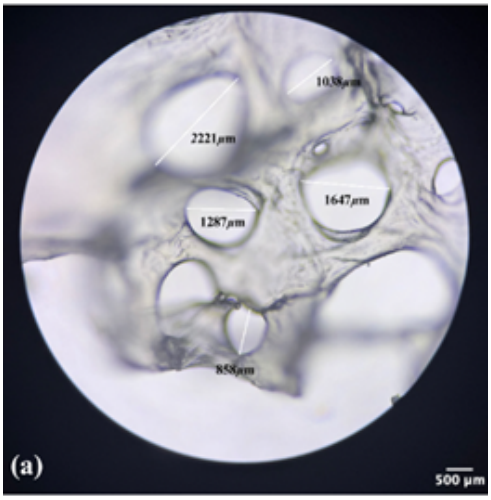

(b)

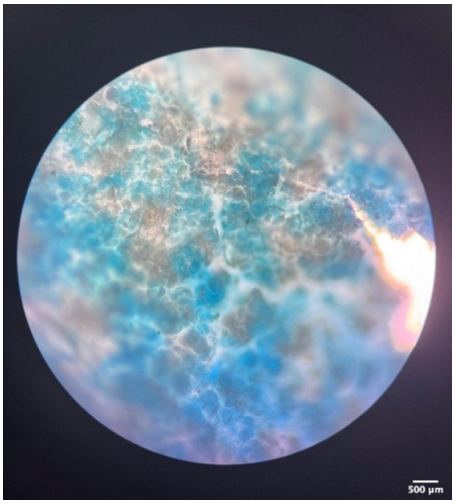

(c)

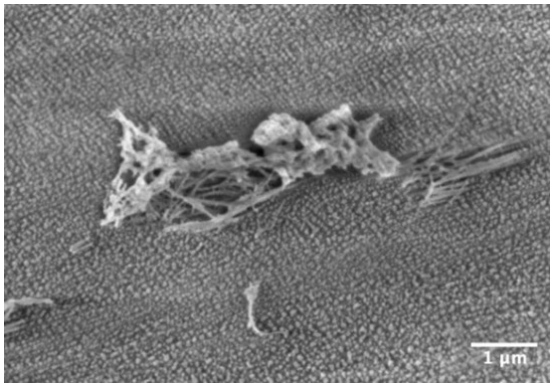

(d)

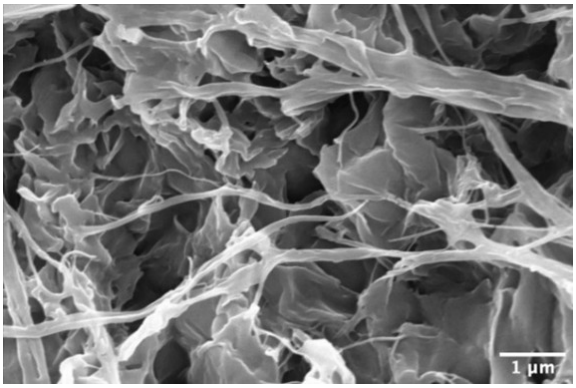

(e)

Figure 4 Porosity and absorption capacity test results. (a) Porosity, blood absorption capacity, and water absorption capacity of the control and tested specimens presented in mean±SE, (b) Light microscopy of the control specimen. (c) Light microscopy of the tested specimen. (d) SEM result of the control specimen. (e) SEM result of the tested specimen

Overall, the tested specimen exhibited an interconnected microfibrillar network with reduced total porosity. The reduced total porosity indicates that DMF-assisted freeze-drying

induces pore wall formation compared with convenient solvent systems, which improves the structural integrity of the scaffold while preserving biologically relevant microporous domains. The resulting hierarchical architecture enhances mechanical stability (Zhang et al., 2025) without compromising the surface characteristics essential for protein adsorption and osteogenic cell attachment (Abbasi, 2020). Accordingly, the observed morphology represents a deliberate structural adaptation that balances mechanical reinforcement with absorption capacities.

The results showed significant differences in its absorption capacities (Figure 4a). The control specimen had higher water absorption capacity (1172.5%±58.63%) and blood absorption capacity (316.6%±15.83%) as compared to the tested specimen (37.7%±1.89%, 29.1%±1.45% respectively).

Table 1 shows the results of blood adhesion tests, where the control specimen have low adhesion ability compared with the tested specimen. This is seen by the amount of blood being transferred from the scaffold to the phosphate-buffered solution, compared to the tested specimen that has merely a small change in the phosphate-buffered solution color. The higher its adhesion ability, reflects a specimen leaning to the ideal bone graft scaffold as it could hold more blood that is absorbed, promoting angiogenesis process and enhanced healing (Sanz et al., 2019).

Table 7 Action plan for improving the supply chain sustainability of Agroindustry B

Specimen Type	Before	After Shaken 10x
Control Specimen	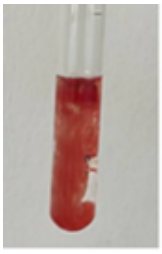	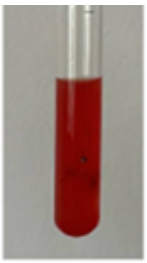
Tested Specimen		

The control specimen has a higher absorption ability because it has larger pores macroscopically. Although it had a lower ability to adhere blood to its scaffold, it still had blood residues that were absorbed homogeneously within the scaffold. On the other hand, the tested specimen whose solid state confirms to have difficulty in absorbing the blood initially showed barely any blood transfer. Notably, the tested specimen only absorbed blood on the white spongy part of the scaffold instead of the solid hard state. Hence, the spongy part may have held more blood and have a higher adhesion ability than its counterpart. The high adhesion ability reflects how it could increase cell attachment to the scaffold, and this is supported by the addition of HAp to the scaffold that could increase cell attachment, proliferation, and differentiation (Biscaia et al., 2022). The scaffold demonstrated controlled absorption capacity, indicating a balance between interconnected porosity and structural stability. The moderate fluid uptake indicates that excessive structural collapse was prevented while sufficient pore accessibility was achieved, likely due to the increased crystallinity observed in XRD analysis.

3.4 Mechanical Testing

The tested specimen demonstrated higher results than the control specimen. The tested specimen (Figure 5a) showed 3.873±0.19 MPa for its ultimate compressive strength and 3.024±0.15 MPa yield strength. Compared with the control specimen (Figure 5b), which resulted in 0.980±0.049 MPa for its ultimate compressive strength and 0.537±0.03 MPa for yield strength.

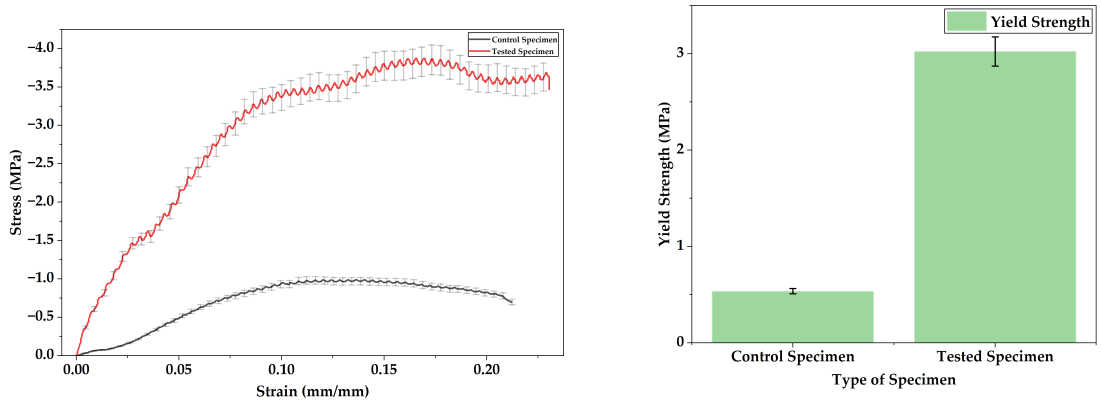

(a) **(b)**

Figure 5 Mechanical test results. (a) Stress-strain curve of the control and tested specimens presented with SE. (b) Yield strength of the control and tested specimen presented in mean ± SE

The higher results could be attributed to the characteristics of the specimen. The control specimen is very porous compared to the tested specimen that showed hard characteristics and a more solid state. A specimen that upholds a higher porous state is known to lean oppositely in its mechanical properties. The higher percentage of HAp in the tested specimen reflects the produced outcome, which is a more compact and harder specimen, increasing its mechanical properties (Juan et al., 2021). In addition, the addition of PCL to the tested specimen indicates the rubbery characteristic of PCL that increases toughness and mechanical strength compared with the control specimen that does not incorporate PCL within the scaffold. This is also supported by the fact that PCL is the slowest to degrade among other polyesters, i.e., PGA > PLGA > PLA > PCL (Dwivedi et al., 2020).

The compressive strength obtained in this study (3.873 MPa) is higher than previously reported β-TCP–PCL freeze-dried scaffolds, which typically range between 1–3 MPa depending on porosity and polymer content (ShiraliPour et al., 2021). The present scaffold shows comparable mechanical performance despite reduced macroporosity. The improvement may be attributed to the higher HAp proportion (60%) and the dense microfibrillar architecture induced by DMF solvent interaction. Its mechanical properties are also within the range of references for an ideal bone graft and is considered to be applicable in the load bearing site. Thus, it could be used in application for dental bone augmentation for socket preservation within load bearing sites (1.5-45 MPa in compressive strength) (Tabatabaee et al., 2023). The control specimen however is still within the range of non-load bearing site (0.1-16 MPa in compressive strength), showing that it could still be used in application for dental bone augmentation (Sunarso et al., 2023).

3.5 Characterization and evaluation of the scaffold properties

The characterization of the tested specimen demonstrated the successful incorporation of organic and inorganic components with distinct physicochemical and mechanical characteristics compared with the control specimen (Table 2).

The FTIR spectrum confirmed the coexistence of phosphate groups from HAp/β-TCP and ester linkages from PCL, while the disappearance of the DMF-specific band at 1670

cm^{-1} indicated complete solvent removal after freeze-drying. XRD analysis identified two main crystalline phases—calcium phosphorus oxide (86.73%) and calcium hydrogen phosphate ($CaHPO_4$, 13.26%)—in the tested specimen, whereas the control specimen exhibited hydroxyapatite (63.36%) and brushite (36.64%) phases. These findings indicate that the type of solvent influences the phase formation and crystalline stability of the composite. Porosity analysis showed a substantial difference between the control specimen (95.79%) and the tested specimen (36.39%), consistent with light microscopy and scanning electron microscopy observations revealing a denser, fibrillar microstructure in the latter. The tested specimen achieved higher compressive (3.873 MPa) and yield strength (3.024 MPa) values than the control (0.980 and 0.537 MPa, respectively), indicating enhanced mechanical integrity. However, its water (37.7%) and blood absorption (29.1%) capacities were significantly lower than those of the control (1172.5% and 316.6%, respectively), suggesting reduced hydrophilicity due to its compact morphology. Nevertheless, the porosity of the tested specimen remains within the generally accepted range for load-bearing bone scaffolds, as reported in previous studies, where moderate porosity is intentionally balanced to achieve higher mechanical stability. Compared with highly porous controls, the current composition demonstrates a favorable trade-off between structural strength and interconnected voids, indicating that the selected HAp–βTCP–PCL-Cu-Zn formulation represents an appropriate and clinically relevant design rather than a porosity deficiency.

Table 2 Summary of significant findings of tested and control specimens

Evaluation	Control Specimen	Tested Specimen
FTIR Spectrum	Presence of collagen type I	Presence of HAp/β-TCP, PCL, and DMF removal
XRD Analysis	Biphasic calcium phosphate	Biphasic calcium phosphate
Porosity (%)	95.79	36.39
Light Microscopy (10x magnification)	Well-defined macropores with a round to oval shape (2539 ± 2047 μm)	Not identifiable (unclear boundary in the image)
SEM Analysis	Micropores 3-5 μm	Micropores <1 μm
Compressive Strength	0.980 MPa	3.873 MPa
Yield Strength	0.537 MPa	3.024 MPa
Water absorption capacity	1172.5%	37.7%
Blood absorption capacity	316.6%	29.1%

Previous studies have generally investigated HAp–PCL or β-TCP–PCL systems separately or without incorporating trace Cu–Zn reinforcement under a DMF-assisted freeze-drying process. This study integrates a 60:40 HAp–β-TCP biphasic composition with PCL and Cu–Zn addition and evaluates its crystallinity, mechanical performance, and absorption behavior in a single framework. This combined physicochemical–mechanical characterization highlights the distinct configuration of the material and supports its positioning at the functional material validation stage.

The evaluation of solvent-related toxicity is essential in this study to ensure the effective removal of dimethylformamide (DMF), which, despite its strong dissolution capability, poses potential cytotoxicity risks. Residual solvents may affect biocompatibility and limit clinical applicability if they are not adequately eliminated. Therefore, Table 3 presents a comparison with prior studies using similar solvent-based fabrication approaches to contextualize how biocompatibility concerns have been addressed and to highlight existing limitations in the field.

Table 3 Comparison of solvent use and biocompatibility considerations in scaffold fabrication studies

Study	Scaffold System	Solvent(s) Used	Method	Biocompatibility Strategy	Results	Toxicity
(ShiraliPour et al., 2021)	β-TCP–PCL scaffold	DMF, DCM	Freeze-drying	Freeze-drying; MTT cell proliferation assay; Live/dead cytotoxicity assay	Increased cell viability with moderate-to-high proliferation	Non-toxic
(Biscaia et al., 2022)	HAp-PCL scaffold	DMF	Solvent casting and melt blending	cell viability assay	Good cell viability and normal cell behavior	Non-toxic
(Cao et al., 2022)	HAp-PCL-multi-walled carbon nanotube scaffold	DMF	3D-printed electro-spinning	CCK-8 assay; Live/dead cytotoxicity assay	Increased cell proliferation and high cell viability with fewer dead cells	Non-toxic
Present study	HAp-β-TCP–PCL–Cu–Zn scaffold	DMF	Freeze-drying	Freeze-drying; FTIR confirmation of solvent removal	No characteristic DMF peaks	Potentially non-toxic; biological validation is needed

Most solvent-based scaffold studies evaluate biocompatibility primarily through post-fabrication biological assays, such as MTT assays or live/dead cytotoxicity assay, while direct verification of residual solvent removal is less frequently reported (Table 3). Although these assays provide important functional insights, they may not fully confirm the absence of cytotoxic solvent residues. FTIR analysis was used to verify solvent removal as an initial validation at the material level. Nevertheless, consistent with prior studies, further in vitro biocompatibility testing remains necessary and is planned in a future study.

4. Conclusions

A biphasic HAp–β-TCP–PCL scaffold reinforced with Cu–Zn was successfully fabricated via a DMF-assisted freeze-drying method and benchmarked against a commercial xenograft control. FTIR analysis verified the presence of phosphate groups from HAp/β-TCP and ester linkages from PCL, while the disappearance of the characteristic DMF band confirmed effective solvent removal. X-ray diffraction (XRD) demonstrated a biphasic calcium phosphate structure dominated by calcium phosphorus oxide with higher crystallinity than the control, indicating that DMF contributed to improved phase formation and structural ordering. Mechanically, the scaffold achieved a compressive strength of 3.873 MPa and a yield strength of 3.024 MPa, surpassing the control and fulfilling the requirements for load-bearing dental applications. Nevertheless, lower porosity (36.39%) and reduced water and blood absorption were observed, which is consistent with the SEM findings of a denser microfibrillar structure with limited pore inter-

connectivity. This work corresponds to the functional material validation stage emphasizing material characterization and functional validation; thus, the scaffold should be considered a functional material candidate. To establish biocompatibility, comprehensive biological and toxicity evaluations, including cytotoxicity, viability, and proliferation assays, are planned for the subsequent development stage.

Acknowledgements

The authors would like to express their gratitude to the Faculty of Medicine and Health Sciences for providing laboratory facilities, technical assistance, and research funding to this research. The authors also acknowledge the assistance of the laboratory staff who contributed to scaffold fabrication and data collection. This research was funded partially by Atma Jaya Catholic University of Indonesia and School of Medicine and Health Sciences Atma Jaya Catholic University of Indonesia, Grant no 1062/III/D.FKIK-KP.104.01/03/2025.

Author Contributions

TO, DN, NM, EU, TD, MO, WW, FR, and DE have contributed to all aspects of this research. All authors took part in giving critical revision of the manuscript. All authors read and approved the final manuscript. The authors declare that there is no conflict of interest regarding the publication of this article. The authors confirmed that the paper was free of plagiarism.

Conflict of Interest

The authors declare no conflicts of interest.

Supplementary Materials

Figure S1 in supplementary file.

References

Abbasi, N. (2020). Porous scaffolds for bone regeneration. *Journal of Science: Advanced Materials and Devices*, *5*(1), 1–9. https://doi.org/10.1016/j.jsamd.2020.01.007

Aboudzadeh, N., Khavandi, A., Javadpour, J., Shokrgozar, M. A., & Imani, M. (2021). Effect of Dioxane and N-Methyl-2-pyrrolidone as a Solvent on Biocompatibility and Degradation Performance of PLGA/nHA Scaffolds. *Iranian Biomedical Journal*, *25*(6), 408–416. https://doi.org/10.52547/ibj.25.6.408

Alberto, L., Kalluri, L., Qu, J., Zhao, Y., & Duan, Y. (2023). Influence of Polycaprolactone Concentration and Solvent Type on the Dimensions and Morphology of Electrosprayed Particles. *Materials*, *16*(5), 2122. https://doi.org/10.3390/ma16052122

Badan Penelitian dan Pengembangan Kesehatan. (2020). *Laporan Nasional Riskesdas 2018*. https://repository.badankebijakan.kemkes.go.id/id/eprint/3514

Basoz, D., Karaman, M. I., Buyuksungur, S., Yucel, D., Hasirci, N., Kocaoglu, B., & Hasirci, V. (2024). 3D printed PCL-nHAp composite implants for the treatment of segmental bone defects: In vivo application in a rabbit model. *Biofabrication*, *17*(1), 015041. https://doi.org/10.1088/1758-5090/ad9fe1

Biscaia, S., Branquinho, M. V., Alvites, R. D., Fonseca, R., Sousa, A. C., Pedrosa, S. S., Caseiro, A. R., Guedes, F., Patrício, T., Viana, T., Mateus, A., Maurício, A. C., & Alves, N. (2022). 3D Printed Poly(e-Caprolactone)/Hydroxyapatite Scaffolds for Bone Tissue Engineering: A Comparative Study on Composite Preparation by Melt Blending or Solvent Casting Techniques and Influence of Bioceramic Content on Scaffold Properties. https://doi.org/10.20944/preprints202201.0221.v1

Callister, W. D., & Rethwisch, D. G. (2020). *Materials Science and Engineering: An Introduction* (10th ed.). Wiley.

Cao, Y., Sun, L., Liu, Z., Shen, Z., Jia, W., Hou, P., & Sang, S. (2022). 3D printed-electrospun PCL/hydroxyapatite/MWCNTs scaffolds for the repair of subchondral bone. *Regenerative Biomaterials*. https://doi.org/10.1093/rb/rbac104

Capuana, E., Lopresti, F., Ceraulo, M., & La Carrubba, V. (2022). Poly-l-Lactic Acid (PLLA)-Based Biomaterials for Regenerative Medicine: A Review on Processing and Applications. *Polymers*, *14*(6), 1153. https://doi.org/10.3390/polym14061153

Chauhan, V., Sharma, S., Maheshwari, R., Juyal, A., Raghuvanshi, S., & Bansal, S. (2009). Evaluation of hydroxyapatite and beta-tricalcium phosphate mixed with bone marrow aspirate as a bone graft substitute for posterolateral spinal fusion. *Indian Journal of Orthopaedics*, *43*(3), 234. https://doi.org/10.4103/0019-5413.49387

Cheng, C., Shie, M.-Y., Lai, Y.-H., Foo, N. P., Lee, M. J., & Yao, C.-H. (2021). Fabrication of 3D Printed Poly(lactic acid)/Polycaprolactone Scaffolds Using TGF-β1 for Promoting Bone Regeneration. *Polymers*, *13*(21), 3731. https://doi.org/10.3390/polym13213731

Choudhury, M., Mohanty, S., & Nayak, S. (2015). Effect of Different Solvents in Solvent Casting of Porous PLA Scaffolds—In Biomedical and Tissue Engineering Applications. *Journal of Biomaterials and Tissue Engineering*, *5*(1), 1–9. https://doi.org/10.1166/jbt.2015.1243

Dwivedi, R., Kumar, S., Pandey, R., Mahajan, A., Nandana, D., Katti, D. S., & Mehrotra, D. (2020). Polycaprolactone as biomaterial for bone scaffolds: Review of literature. *Journal of Oral Biology and Craniofacial Research*, *10*(1), 381–388. https://doi.org/10.1016/j.jobcr.2019.10.003

Figueiredo, M. M., Gamelas, J. A. F., & Martins, A. G. (2012). Characterization of Bone and Bone-Based Graft Materials Using FTIR Spectroscopy. In *Infrared spectroscopy - life and biomedical sciences*. https://doi.org/10.5772/36379

Gasner, N. S., & Schure, R. S. (2023). Periodontal Disease. https://ncbi.nlm.nih.gov/books/NBK554590/

Ghezzi, B., Matera, B., Meglioli, M., Rossi, F., Duraccio, D., Faga, M. G., Zappettini, A., Macaluso, G. M., & Lumetti, S. (2024). Composite PCL Scaffold With 70% β-TCP as Suitable Structure for Bone Replacement. *International Dental Journal*. https://doi.org/10.1016/j.identj.2024.02.013

Hajishengallis, G., & Chavakis, T. (2021). Local and systemic mechanisms linking periodontal disease and inflammatory comorbidities. *Nature Reviews Immunology*, *21*(7). https://doi.org/10.1038/s41577-020-00488-6

Hashimoto, K., Oikawa, H., & Shibata, H. (2024). Characterization of Porous β-Type Tricalcium Phosphate Ceramics Formed via Physical Foaming with Freeze-Drying. *International Journal of Molecular Sciences*, *25*(10), 5363. https://doi.org/10.3390/ijms25105363

Jain, N., Dutt, U., Radenkov, I., & Jain, S. (2023). WHO's global oral health status report 2022: Actions, discussion, & implementation. *Oral Diseases*, *30*(2). https://doi.org/10.1111/odi.14516

Jang, I.-N., & Ahn, Y.-S. (2023). The Study of Copper Powder Sintering for Porous Wick Structures with High Capillary Force. *Materials*, *16*(12), 4231. https://doi.org/10.3390/ma16124231

Juan, P.-K., Fan, F., Lin, W.-C., Liao, P.-B., Huang, C. C., Shen, Y. K., Ruslin, M., & Lee, C.-H. (2021). Bioactivity and Bone Cell Formation with Poly-ε-Caprolactone/Bioceramic 3D Porous Scaffolds. *Polymers*, *13*(16), 2718. https://doi.org/10.3390/polym13162718

Keum, B.-R., Kim, H. J., Kim, G.-H., & Chang, D.-G. (2023). Osteobiologies for Spinal Fusion from Biological Mechanisms to Clinical Applications: A Narrative Review. *International Journal of Molecular Sciences*, *24*(24), 17365. https://doi.org/10.3390/ijms242417365

Kono, T., Sakae, T., Nakada, H., Kaneda, T., & Okada, H. (2022). Confusion between Carbonate Apatite and Biological Apatite (Carbonated Hydroxyapatite) in Bone and Teeth. *Minerals*, *12*(2), 170. https://doi.org/10.3390/min12020170

Kumar, V. (2024). Influence of ligand field strength on the kinetics of transition metal-catalyzed reactions. *International Journal of Chemical Studies*, *12*(5), 65–69. https://doi.org/10.22271/chemi.2024.v12.i5a.12440

Kwon, T., Lamster, I. B., & Levin, L. (2020). Current Concepts in the Management of Periodontitis. *International Dental Journal*, *71*(6), 462–476. https://doi.org/10.1111/idj.12630

Lee, S. W., Kim, Y., Rho, H. T., & Kim, S. (2022). Microhardness and microstructural properties of a mixture of hydroxyapatite and β-tricalcium phosphate. *Journal of Asian Ceramic Societies*, *11*(1), 11–17. https://doi.org/10.1080/21870764.2022.2136261

Lv, N., Zhou, Z., Hong, L., Li, H., Liu, M., & Qian, Z. (2024). Zinc-energized dynamic hydrogel accelerates bone regeneration via potentiating the coupling of angiogenesis and osteogenesis. *Frontiers in Bioengineering and Biotechnology*, *12*. https://doi.org/10.3389/fbioe.2024.1389397

Manalu, F. R. G., & Basuki, W. W. (2025). Rancang Bangun Alat Uji Kekuatan Material Polimer dan Komposit Polimer Berpenguat Serat Alam. *Cylinder: Jurnal Ilmiah Teknik Mesin*, *11*(1). https://doi.org/10.25170/cylinder.v11i1.6648

Mondal, S., Park, S., Choi, J., Thu, T., Doan, M., Vo, T., Lee, B., & Oh, J. (2023). Hydroxyapatite: A journey from biomaterials to advanced functional materials. *Advances in Colloid and Interface Science*, *321*, 103013. https://doi.org/10.1016/j.cis.2023.103013

Muzart, J. (2009). N,N-Dimethylformamide: Much more than a solvent. *Tetrahedron*, *65*(40), 8313–8323. https://doi.org/10.1016/j.tet.2009.06.091

NOAA. (n.d.). Dimethylformamide DMF Cautionary Response Information. https://cameochemicals.noaa.gov/chris/DMF.pdf

Ntrivala, M. A., Pitsavas, A. C., Lazaridou, K., Baziakou, Z., Karavasili, D., Papadimitriou, M., Ntagkopoulou, C., Balla, E., & Bikiaris, D. N. (2025). Polycaprolactone (PCL): The biodegradable polyester shaping the future of materials – a review on synthesis, properties, biodegradation, applications and future perspectives. *European Polymer Journal*, *234*, 114033. https://doi.org/10.1016/j.eurpolymj.2025.114033

Obregon, N., Agubra, V., Pokhrel, M., Campos, H., Flores, D., De, D., Mao, Y., Macossay, J., & Alcoutlabi, M. (2016). Effect of Polymer Concentration, Rotational Speed, and Solvent Mixture on Fiber Formation Using Forcespinning®. *Fibers*, *4*(4), 20. https://doi.org/10.3390/fib4020020

Omiyale, B. O., Ogbeyemi, A., Rasheed, A. A., Adamolekun, T. M., & Zhang, W. C. (2025). Influence of electrospinning parameters on the development of high-quality electrospun nanofibers: A brief critical assessment. *Next Nanotechnology*, *8*, 100295. https://doi.org/10.1016/j.nxnano.2025.100295

Prasadh, S., & Wong, R. C. W. (2018). Unraveling the mechanical strength of biomaterials used as a bone scaffold in oral and maxillofacial defects. *Oral Science International*, *15*(2), 48–55. https://doi.org/10.1016/S1348-8643(18)30005-3

Purnaning, D., Hurnah, H., Taufik S, A., Rahayu, S., Kurniawidi, D. W., & Hadi, K. A. (2025). Influence of Composition and Lypholization Time on Physical Properties of HA/Cs/Coll/Hydroxypropyl Methylcellulose Biocomposites for Bone Graft Scaffolds. *Indonesian Physical Review*, *8*(2), 616–628. https://doi.org/10.29303/ipr.v8i2.474

Ragu, A., Senthilarasan, K., & Sakthivel, P. (2015). Synthesis and Characterization of Nano Hydroxyapatite with Polyoxymethylene Nanocomposites for Bone Growth Studies. *International Journal of Scientific Engineering and Research*, *3*(7), 120–123. https://doi.org/10.70729/ijser15353

Raja, N., Oktawati, S., Setiawati, D., Rukmana, A., & Endang, S. (2022). Socket Preservation Using Bovine Bone Graft and Pericardium Membrane: A Case Report. *KnE Medicine*, 54–60. https://doi.org/10.18502/kme.v2i1.10837

Ratajczyk, P., Sobczak, S., & Katrusiak, A. (2018). High-Pressure Structure and Properties of N,N-Dimethylformamide (DMF). *Crystal Growth & Design*, *19*(2), 896–901. https://doi.org/10.1021/acs.cgd.8b01452

Rozykulyyeva, L., Widiyanti, P., & Astuti, S. D. (2025). Pomegranate-peel-chitosan-gelatin composite: A hemostatic dental sponge with antibacterial enhancement. *Dental Journal*, *58*(2), 171–179. https://doi.org/10.20473/j.djmkg.v58.i2.p171-179

Sanz, M., Dahlin, C., Apatzidou, D., Artzi, Z., Bozic, D., Calciolari, E., De Bruyn, H., Dommisch, H., Donos, N., Eickholz, P., Ellingsen, J. E., Haugen, H. J., Herrera, D., Lambert, F., Layrolle, P., Montero, E., Mustafa, K., Omar, O., & Schliephake, H. (2019). Biomaterials and regenerative technologies used in bone regeneration in the craniomaxillofacial region: Consensus report of group 2 of the 15th European Workshop on Periodontology on Bone Regeneration. *Journal of Clinical Periodontology*, *46*, 82–91. https://doi.org/10.1111/jcpe.13123

ShiraliPour, F., Shafiei, S. S., & Nikakhtar, Y. (2021). Three-dimensional porous poly(ε-caprolactone)/beta-tricalcium phosphate microsphere-aggregated scaffold for bone tissue engineering. *International Journal of Applied Ceramic Technology*, *18*(5), 1442–1456. https://doi.org/10.1111/ijac.13770

Sunarso, S., Suryadi, A., Indrani, D. J., & Pangesty, A. I. (2023). Compressive Strength of Newly Developed Nonsintered Hydroxyapatite Blocks for Bone Graft Applications. *European Journal of Dentistry*, *18*(03), 815–819. https://doi.org/10.1055/s-0043-1774327

Tabatabaee, S., Delyanee, M., Samanipour, R., & Tavakoli, A. (2023). The potential of the mineralized bone allograft block as an appropriate candidate for bone tissue engineering in periodontology. *Journal of Materials Research*, *38*(20), 4497–4508. https://doi.org/10.1557/S43578-023-01166-8

Tan, Z., Zhou, B., Zheng, J., Huang, Y., Zeng, H., Xue, L., & Wang, D. (2021). Lithium and Copper Induce the Osteogenesis-Angiogenesis Coupling of Bone Marrow Mesenchymal Stem Cells via Crosstalk between Canonical Wnt and HIF-1α Signaling Pathways. *Stem Cells International*, 1–15. https://doi.org/10.1155/2021/6662164

Taufik, A., Zuhan, A., Kusdaryono, S., & Rohadi, R. (2017). Karakterisasi Hydroxyapatite Alami yang dibuat dari Tulang Sapi dan Cangkang Telur sebagai Bahan untuk Donor Tulang (Bone Graft). *Unram Medical Journal*, *6*(1). https://doi.org/10.29303/jku.v6i1.33

Veiga, A., Madureira, S., Costa, J. B., Castro, F., Rocha, F., & Oliveira, A. L. (2023). Tackling current production of HAp and HAp-driven biomaterials. *Materials Advances*, *4*(22), 5453–5478. https://doi.org/10.1039/D3MA00363A

Wang, H., Yuan, L., & An, J. (2017). Crystallographic Characteristics of Hydroxylapatite in Hard Tissues of Cololabis saira. *Crystals*, *7*(4), 103. https://doi.org/10.3390/cryst7040103

Wen, X., Wang, J., Pei, X., & Zhang, X. (2023). Zinc-based biomaterials for bone repair and regeneration: Mechanism and applications. *Journal of Materials Chemistry B*, *11*(48), 11405–11425. https://doi.org/10.1039/D3TB01874A

Zhang, J., Li, J., & Guan, W. (2025). Photocatalytic Hydrogen Production Performance of ZnCdS/$CoWO_4$ Heterojunctions in the Reforming of Lignin Model Compounds. *Materials*, *18*(18), 4401. https://doi.org/10.3390/ma18184401

Zhao, R., Yang, R., Cooper, P. R., Khurshid, Z., Shavandi, A., & Ratnayake, J. (2021). Bone Grafts and Substitutes in Dentistry: A Review of Current Trends and Developments. *Molecules*, *26*(10), 3007. https://doi.org/10.3390/molecules26103007